The Effect of Annealing Temperature on Statistical Properties of WO_3 Surface

G. R. Jafari [a,b], A. A. Saberi [c], R. Azimirad [c], A. Z. Moshfegh [c], and S. Rouhani [c]
[a] *Department of Physics, Shahid Beheshti University, Evin, Tehran 19839, Iran*
[b] *Department of Nano-Science, IPM, P. O. Box 19395-5531, Tehran, Iran*
[c] *Department of Physics, Sharif University of Technology, P.O. Box 11365-9161, Tehran, Iran*

We have studied the effect of annealing temperature on the statistical properties of WO_3 surface using atomic force microscopy techniques (AFM). We have applied both level crossing and structure function methods. Level crossing analysis indicates an optimum annealing temperature of around 400^oC at which the effective area of the WO_3 thin film is maximum, whereas composition of the surface remains stoichiometric. The complexity of the height fluctuation of surfaces was characterized by roughness, roughness exponent and lateral size of surface features. We have found that there is a phase transition at around 400^oC from one set to two sets of roughness parameters. This happens due to microstructural changes from amorphous to crystalline structure in the samples that has been already found experimentally.

arXiv:0704.1023v1 [physics.data-an] 8 Apr 2007

I. INTRODUCTION

Transition metal oxides represent a large family of materials possessing various interesting properties, such as superconductivity, colossal magneto-resistance and piezoelectricity. Among them, tungsten oxide is of intense interest and has been investigated extensively for its distinctive properties. With outstanding electrochromic [1, 2, 3, 4, 5, 6], photochromic [7], gaschromic [8], gas sensor [9, 10, 11], photo-catalyst [12], and photoluminescence properties [13], tungsten oxide has been used to construct "smart-window", anti-glare rear view mirrors of automobile, non-emissive displays, optical recording devices, solid-state gas sensors, humidity and temperature sensors, biosensors, photonic crystals, and so forth.

WO_3 thin films can be prepared by various deposition techniques such as thermal evaporation [3, 8], spray pyrolysis [14], sputtering [6], pulsed laser ablation [10, 11], sol-gel coating [2, 5, 15], and chemical vapor deposition [16].

The gas sensitivity of WO_3 heavily depends upon film parameters such as composition, morphology (e.g. grain size), nanostructure and microstructure (e.g. porosity, surface-to-volume ratio). Film parameters are related to the deposition technique used, the deposition conditions and the subsequent annealing process. Annealing, which is an essential process to obtain stable films with well-defined microstructure, causes stoichiometry and microstructural changes that have a high influence on the sensing characteristics of the films [17]. Moreover, the surface structure and surface morphology of the metal oxides are also important for different applications. In fact, the electrochromic devices are made of amorphous oxides [1], while crystalline phase plays a major role in catalysts and sensors [17]. This is because, the minor change in their chemical composition and crystalline structure could modify different properties of the metal oxides.

In practice, one of the effective ways to modify the surface morphology is annealing process at various temperatures. So far, most of morphological analysis related to the WO_3 surface were accessible through the experimental methods. Usually these analysis are rigorous and time consuming. Moreover, lack of the suitable analysis for AFM data to find the nano and microstructural properties of surfaces was feeling perfectly.

In this article, we introduce the methods: roughness analysis and level crossing as suitable candidates and show that we can get easily the structure and morphological properties of a surface in a fast manner, only using the AFM observation as an initial data.

The roughness of a surface has been studied as a simple growth model using analytical and numerical methods [18, 19, 20, 21, 22, 23, 24, 25, 26]. These studies quite generally proposed that the height fluctuations have a self-similar character and their average correlations exhibit a dynamic scaling form. Also some authors recently use the average frequency of positive slope level crossing to provide further complete analysis on roughness of a surface [27]. This stochastic approach has turned out to be a promising tool also for other systems with scale dependent complexity, such as in surface growth where one would like to measure the roughness [28]. Some authors have applied this method to study the fluctuations of velocity fields in Burgers turbulence [29] and the Kardar-Parisi-Zhang equation in (d+1)-dimensions [30] and analyzing the stock market [31].

In this work, we have used the scaling analysis to determine the roughness, roughness exponent and the lateral size of surface features. Moreover, level crossing analysis has been utilized to estimate the effective area of a surface.

This paper is organized as follows: In section II, we have discussed about the film preparation and experi-

mental results obtained from AFM, XPS and UV-visible spectrophotometer for the annealed samples at the various temperatures. In section III, we have introduced the analytical methods briefly. Data description and data analysis based on the statistical parameters of WO_3 surface as a function of annealing temperatures are given in section IV.Finally, section V concludes presented results.

II. EXPERIMENTALS

Thin films of WO_3 were deposited on microscope slide glass using thermal evaporation method. The deposition system was evacuated to a base pressure of $\sim 4\times10^{-3}Pa$. Thickness of the deposited films was considered about 200 nm measured by the stylus and optical techniques. More details about the other deposition parameters of the films are recently reported elsewhere [32].

To study the effect of annealing temperature on surface structure and optical properties of the samples, they were annealed at 200, 300, 350, 400, 450, and 500^oC in air for a period of 60 min. Optical transmission and reflection measurements of the deposited films were performed in a range of 300-1100 nm wavelength using a Jascow V530 ultraviolet (UV)-visible spectrophotometer with resolution of 1 nm.

X-ray photoelectron spectroscopy (XPS) using a Specs EA 10 Plus concentric hemispherical analyzer (CHA) with $Al\ K_\alpha$ anode at energy of 1486.6 eV was employed to study the atomic composition and chemical state of the tungsten oxide thin films. The pressure in the ultra high vacuum surface analysis chamber was less than $1.0\times10^{-7}Pa$. All binding energy values were determined by calibration and fixing the $C(1s)$ line to 285.0 eV. The XPS data analysis and deconvolution were performed by SDP (version 4.0) software. The nanoscale Surface topography of the deposited films was investigated by Thermo Microscope Autoprobe CP-Research atomic force microscopy (AFM) in air with a silicon tip of 10 nm radius in contact method. The AFM images were recorded with resolution of about 20 nm in a scale of $5\times5\ \mu m$.

A. XPS Characterization

The elemental and chemical characterizations of the films were performed by XPS. Figure 1a shows the $W(4f)$ core level spectra recorded on the "as deposited" WO_3 sample, and the results of its fitting analysis. To reproduce the experimental data, one doublet function was used for the $W(4f)$ component. This contains $W(4f_7/2)$ at 35.6 eV and $W(4f_5/2)$ at 37.8 eV with a full-width at half-maximum (FWHM) of $1.75\pm0.04\ eV$. The area ratio of these two peaks is 0.75 which is supported by the spin-orbit splitting theory of $4f$ levels. Moreover, the structure was shifted by 5 eV toward higher energy

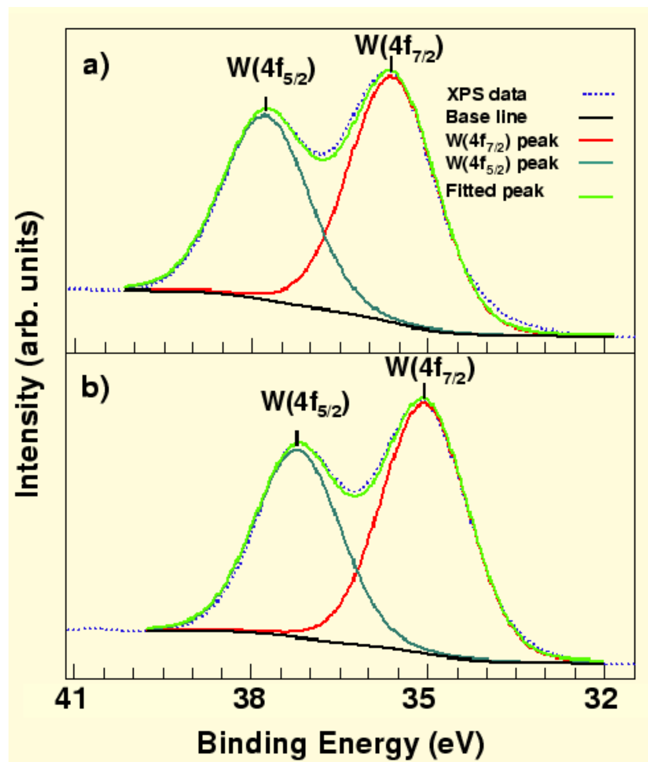

FIG. 1: $W(4f)$ core level spectra of WO_3 thin films: a) "as deposited" and b) annealed at 500^oC.

relative to the metal state.
It is thus clear that the main peaks in our XPS spectrum attributed to the W^{6+} state on the surface [1, 2, 33]. In stoichiometric WO_3, the six valence electrons of the tungsten atom are transferred into the oxygen p-like bands, which are thus completely filled. In this case, the tungsten $5d$ valence electrons have no part of their wave function near the tungsten atom and the remaining electrons in the tungsten atom experience a stronger Coulomb interaction with the nucleus than in the case of tungsten atom in a metal, in which the screening of the nucleus has a component due to the $5d$ valence electrons. Therefore, the binding energy of the $W(4f)$ level is larger in WO_3 than in metallic tungsten. If an oxygen vacancy exists, the electronic density near its adjacent W atom increases, the screening of its nucleus is higher and, thus, the $4f$ level energy is expected to be at lower binding energy [1].

By increasing the annealing temperature it was observed that the position of $W(4f)$ peak did not obviously change. But for WO_3 thin film annealed at 500^oC (Fig. 1b), the $W(4f)$ peak moved to a lower binding energy so that $W(4f_{7/2})$ position was observed at 35.0 eV. This can be related to oxygen vacancy at this high annealing temperature and formation of W^{5+}.

B. Optical Characterization

The transmittance and reflectance spectra in the visible and infrared range recorded for the WO_3 thin films before and after annealing at different temperatures (Fig. 2a). It is seen that, the transmittance of the "as deposited" films in the visible range varies from about 80 up to nearly 100% (without considering the substrate contribution). Correspondingly, maximum value of the reflectance for both the film and the substrate is about 20% (the reflectance from the bare glass substrate was measured about 10%). The sharp reduction in the transmittance spectrum at the wavelength of $\sim 350nm$ is due to the fundamental absorption edge that was also reported previously [1, 2, 3].
The oscillations in the transmission and reflection spectra are caused by optical interference. The optical transmittance of WO_3 films strongly depends on the oxygen content of the films. In fact, non-stoichiometric films with composition of WO_{3-x} show a blue tinge for $x > 0.03$ [34].
The "as deposited" pure tungsten oxide films were highly transparent with no observable blue coloration, under our experimental conditions. As can be seen from Fig. 2a after annealing process at 200 to 400^oC, the transmittance and reflectance of the WO_3 films have not changed significantly. Only, the position of the oscillations altered due to thickness reduction and film condensation after the heat-treatment process [1]. At 500^oC transmittance and reflectance of the annealed WO_3 film is reduced about 10%, therefore at this temperature, the film turn into non-stoichiometric composition, so that it could be seen from changing color of the film.

The optical gap (E_g) was evaluated from the absorption coefficient (α) using the standard relation: $(\alpha h\nu)^{1/\eta} = A(h\nu - E_g)$, in which η depends on the kind of optical transition in semiconductors, and α was determined near the absorption edge using the simple relation: $\alpha = ln[(1-R)^2/T]/d$,where d is thickness of the film. More useful explanation about the optical band gap calculation reported in [32]. The relationship between the optical band gap energy and annealing temperature for WO_3 thin films has been shown in Fig. 2b. As can be seen from it, the optical band gap for the "as deposited" WO_3 evaluated 3.4 eV. Amorphous structure of the "as deposited" WO_3 causes to E_g is bigger than 2.7 eV. After annealing samples at 200 and 300^oC, the optical band gap decreased slightly about 0.1 eV which can be related to condensation of the films. But the optical band gap of the WO_3 annealed at 400^oC reduced to 3.1 eV due to crystallization of the film. This reduction continues to 2.5 eV for the sample annealed at 500^oC. Reason of the E_g becomes smaller than 2.7 eV is oxygen vacancy at this temperature as was seen in Fig 1b. It is to note that for evaporated WO_3 films one has found $2.7 < E_g < 3.5$ eV [1].

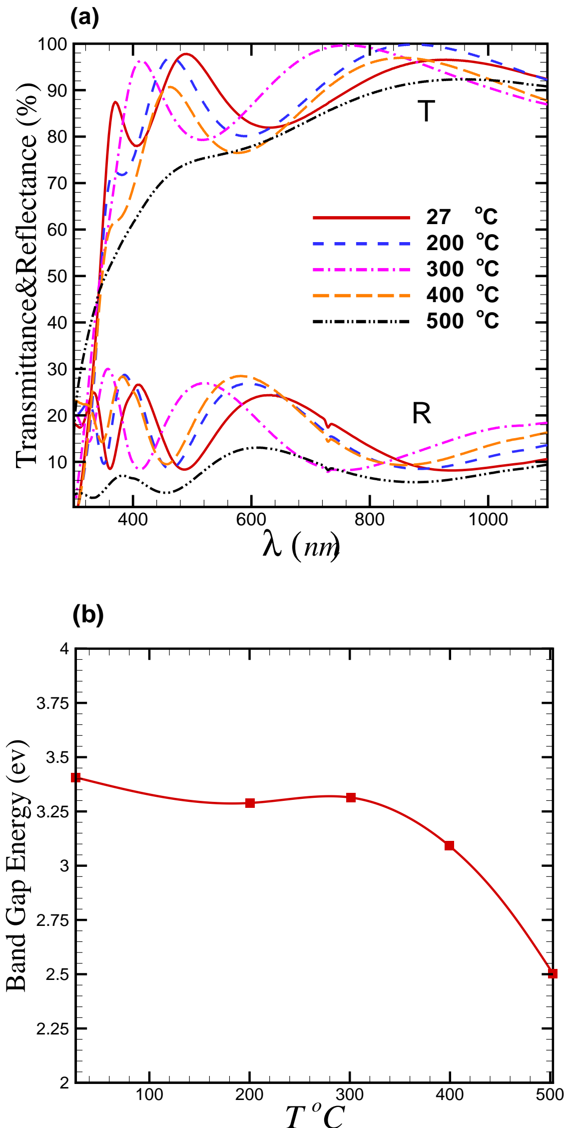

FIG. 2: a) Optical transmittance (T) and reflectance (R) and b) Optical band gap energy of the WO_3 thin films annealed at different temperatures.

C. AFM Analysis

To study the effect of the annealing process on the surface morphology of the films, we have shown AFM images of the WO_3 surfaces annealed at the different temperatures : 200, 300, 350, 400, 450, 500^oC in Figure 1. As can be seen from Fig. 1, for the annealed film at 200^oC, it seems that the surface morphology of the film is relatively the same with a smooth surface, amorphous structure and nanometric grain size, as also reported by other investigators for WO_3 films [35, 36]. We have also ob-

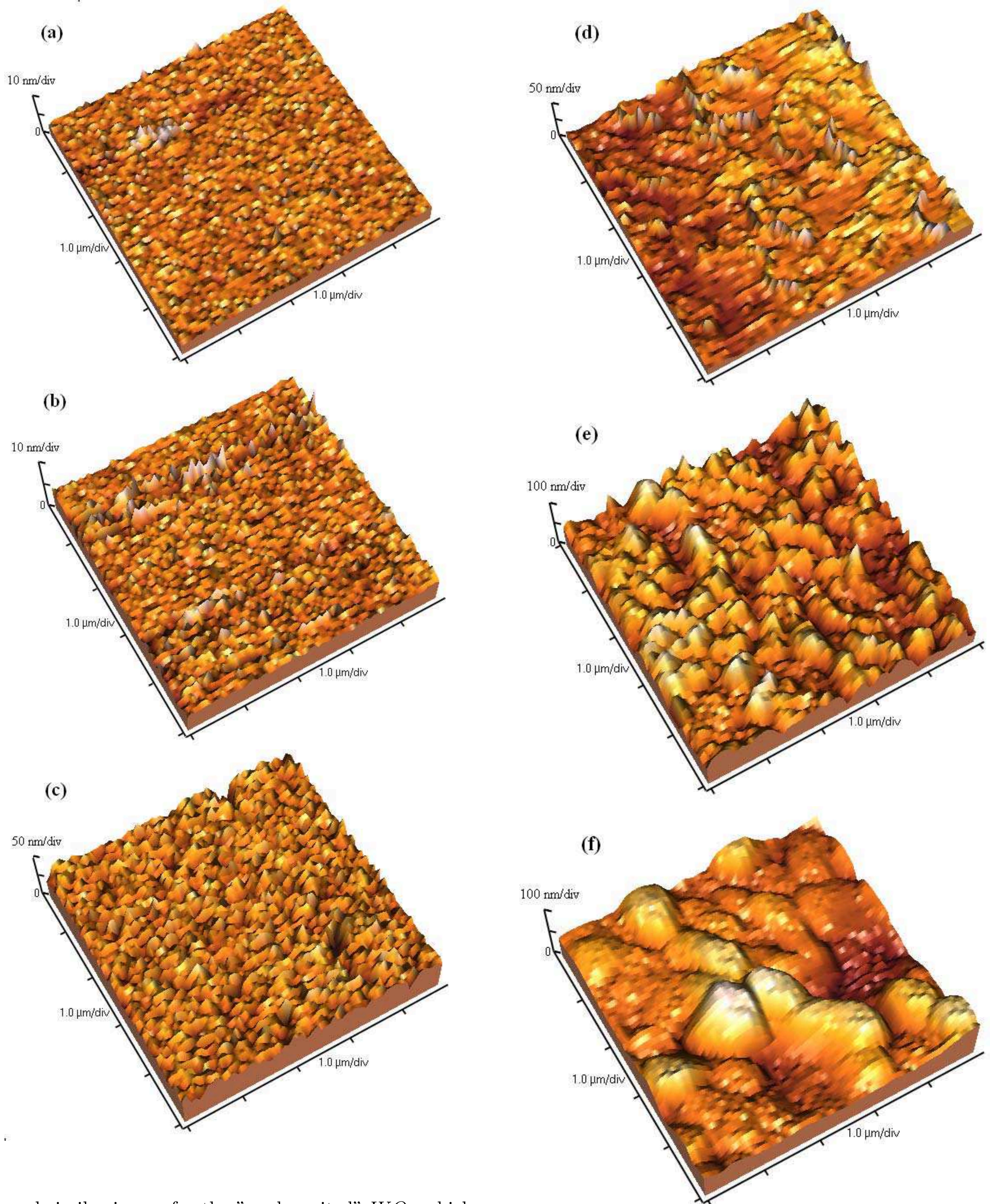

served similar image for the "as deposited" WO_3 which is not shown here. For WO_3 thin films, increasing annealing temperature to 350^oC did not significantly effect on surface parameters because it is low temperature for crystallization of WO_3 [1]. But at higher annealing temperatures 400, 450 and 500^oC, surface grain size and

FIG. 3: AFM images of WO_3 thin films annealed at various temperatures a) 200, b) 300, c) 350, d) 400, e) 450 and f) 500^oC, respectively.

roughness begin to increase. The more precise analysis of these surfaces are given in the next section.

III. STATISTICAL QUANTITIES

A. Roughness Analysis

It is also known that to derive the quantitative information of the surface morphology one may consider a sample of size L and define the mean height of growing film $\overline{h}$ and its roughness σ by:

$$\sigma(L,t) = (\langle (h-\overline{h})^2 \rangle)^{1/2} \tag{1}$$

where t is growing time and $\langle \cdots \rangle$ denotes an averaging over different samples, respectively. Moreover, growing time is a factor which can be applied to control the surface roughness of thin films.

Let us now calculate the roughness exponent of the growing surface. Starting from a flat interface (one of the possible initial conditions), it is conjectured that a scaling of lenght by factor b and of time by factor b^z (z is the dynamical scaling exponent), rescales the roughness σ by factor b^χ as follows [18]:

$$\sigma(bL, b^z t) = b^\alpha \sigma(L,t) \tag{2}$$

which implies that

$$\sigma(L,t) = L^\alpha f(t/L^z). \tag{3}$$

For large t and fixed L ($i.e. x = t/L^z \to \infty$) σ saturate. However, for fixed and large L and $t \ll L^z$, one expects that correlations of the height fluctuations are set up only within a distance $t^{1/z}$ and thus must be independent of L. This implies that for $x \ll 1$, $f(x) \sim x^\beta g'(\lambda)$ with $\beta = \alpha/z$. Thus, dynamic scaling postulates that

$$\sigma(L,t) = \begin{cases} t^\beta, & \text{t} \ll L^z; \\ L^\alpha, & \text{t} \gg L^z. \end{cases} \tag{4}$$

The roughness exponent α and the dynamic exponent β characterize the self-affine geometry of the surface and its dynamics, respectively. In the present work, we see the surfaces at the limit $t \to \infty$ and so we will only obtain the α exponent.

The common procedure to measure the roughness exponent of a rough surface is use of the surface structure function depending on the length scale l which is defined by :

$$S^2(l) = \langle |h(x+l) - h(x)|^2 \rangle. \tag{5}$$

It is equivalent to the statistics of height-height correlation function $C(l)$ for stationary surfaces, i.e. $S^2(l) = 2\sigma^2(1 - C(l))$. The second order structure function $S^2(l)$, scales with l as $l^{2\alpha}$.

B. Level Crossing Analysis

Let ν_α^+ denotes the number of positive slope crossing of $h(x) - \bar{h} = \alpha$ for interval L.

Since the process is homogeneous, if we take a second time interval of L immediately following the first we shall obtain the same result, and for two intervals together we shall therefore obtain [28]:

$$N_\alpha^+(2L) = 2N_\alpha^+(L), \tag{6}$$

from which it follows that, for a homogeneous process, the average number of crossing is proportional to the interval L. Hence

$$N_\alpha^+(L) \propto L, \tag{7}$$

or

$$N_\alpha^+(L) = \nu_\alpha^+ L, \tag{8}$$

where ν_α^+ is the average frequency of positive slope crossing of the level $h(x) - \bar{h} = \alpha$. We now consider how the frequency parameter ν_α^+ can be deduced from the underlying probability distributions for $h(x) - \bar{h}$.

Consider a small length scale δx of a typical sample function. Since we are assuming that the process $h(x) - \bar{h}$ is a smooth function of x, with no sudden ups and downs, if δx is small enough, the sample can only cross $h(x) - \bar{h} = \alpha$ with positive slope if $h(x) - \bar{h} < \alpha$ at the beginning of the interval L. Furthermore, there is a minimum slope at x if the level $h(x) - \bar{h} = \alpha$ is to be crossed in interval Δx depending on the value of $h(x) - \bar{h}$ at position x. So there will be a positive crossing of $h(x) - \bar{h} = \alpha$ in the next interval Δx if, at x,

$$h(x) - \bar{h} < \alpha \quad \text{and} \quad \frac{\Delta\left[h(x) - \bar{h}\right]}{\Delta x} > \frac{\alpha - \left[h(x) - \bar{h}\right]}{\Delta x}. \tag{9}$$

As shown in [28], the frequency ν_α^+ can be written in terms of joint PDF (probability distribution function) of $p(\alpha, y')$ as follows:

$$\nu_\alpha^+ = \int_0^\infty p(\alpha, y') y' dy'. \tag{10}$$

and then the quantity N_{tot}^+ which is defined as:

$$N_{tot}^+ = \int_{-\infty}^{+\infty} \nu_\alpha^+ |\alpha - \bar{\alpha}| d\alpha. \tag{11}$$

will measure the total number of crossing the surface with positive slope. So, the N_{tot}^+ and square area of growing surface are in the same order. Concerning this, it can be utilized as another quantity to study further the roughness of a surface [27].

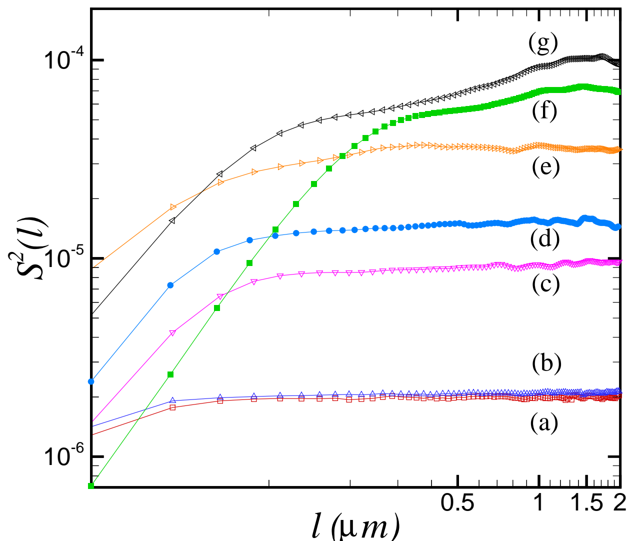

FIG. 4: Log-Log plot of the selection structure function of various annealed temperature: a) 27, b) 200, c) 300, d) 350, e) 400, f) 450, g) 500^oC.

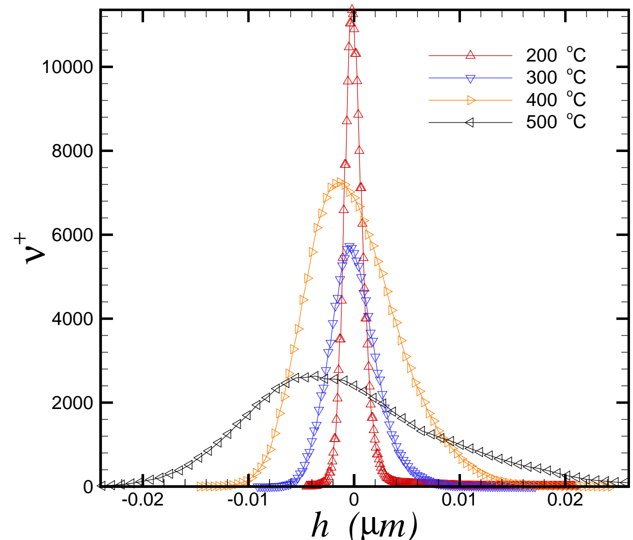

FIG. 5: The average frequency ν_α^+ as a function of height h

IV. RESULTS AND DISCUSSION

Thin films of WO_3 were deposited by using thermal evaporation method and then surface micrographs of WO_3 samples were obtained by AFM technique after annealed at different temperatures (Fig.3).
These micrographs were then analyzed using methods from stochastic data analysis have introduced in the last section. Figure 3 shows AFM images of WO_3 thin films annealed at 200 ,300 ,350 ,400 ,450, and 500^oC. The "as deposited" and annealed sample at 200^oC (Fig. 3a) have columnar structure, indicating that up to 200^oC no significant changes in the microstructure occurs. However, at higher temperatures (figs. 3b-3f) we have observed increased grain size and rougher surface. Specifically at 500^oC (Fig. 3f) we observe stark changes in the micrograph which is accompanied by composition changes in the surface. This can be related to the phase transition to Magneli phase e.g. WO_{3-x} in the annealing process [36]. This is also confirmed by our XPS and UV-visible spectrophotometry analysis (Sec. II). These are shown the significant formation of W^{5+} state in the surface at 500^oC.

Also our analysis shows that below 400^oC the surfaces are in amorphous phase with the same behavior for all scales, but as soon as the crystalline phase appears the system behaves differently which diagnostics at small and large scale for temperatures above 400^oC. By using parameters of the analytical method given here, these transitions can be quantified.

Now, we will use the statistical parameters introduced in the last section and will obtain some quantitative information about the effect of annealing temperature on the surface topography of the WO_3 samples.

The structure function $S^2(l)$ as defined in Eq.(5) can be used to quantify the topology of a rough surface. The structure function $S^2(l)$ is plotted against the length scale of the sample in Fig.4 . The saturated $S^2(l)$ is an indication of the surface roughness, as $2\sigma^2$. The most obvious observation indicates that roughness is raised with increasing annealing temperature. Roughness has a minimum of $0.91nm$ at 27 and 200^oC and a maximum of $48nm$ at 500^oC. This is because higher temperatures create higher peaks (i.e. peaks with more deviations from the average) . All exponents which is derivable from $S^2(l)$ have been summarized and given in Table I.

As depicted in Fig.4 , the structure function $S^2(l)$, has a different behavior in the various temperatures. So that, in the annealing temperature range 27-350^oC it has a typical behavior in all scales, but in the higher temperature range 400-500^oC its behavior is different in the small and large scales. In the other words, the phase transition is occurred at 400^oC, because for higher temperatures, there are two sets of roughness parameters needed to simulate the surface morphology. It can be related to the phase transition in the structure of the surface from amorphous to crystalline phase has been yielded from the band gap energy (see the section II.B).

The slope of each $S^2(l)$ curves at the small and large scales yields the roughness exponents α and α' of

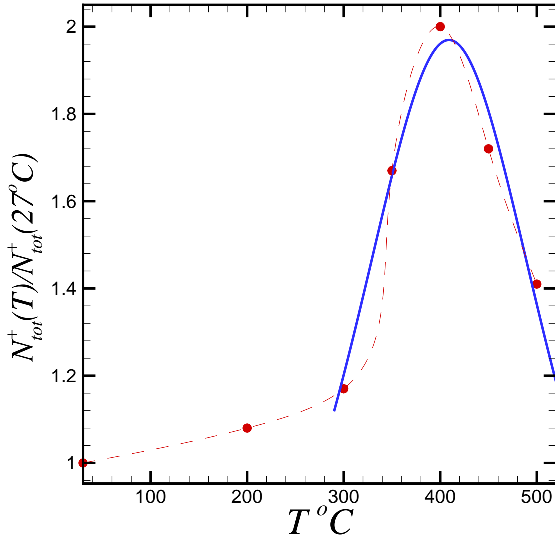

FIG. 6: The normalized N^+_{tot} behavior as a function of annealing temperature. The solid line is plotted according to Eq.(12) around 400^oC .

the corresponding surface. Hence, it is seen that the mono roughness exponent increases with the addition of annealing temperature up to 400^oC. In the higher temperatures, we have obtained two roughness exponents(α-α') equal to the 0.40-0.14, 0.71-0.20, and 0.69-0.24 for temperatures 400, 450 and 500^oC, respectively. Difference in the α values, in these temperatures, are in agreement with changes of correlation length. Where the correlation length, is the distance at which the structure function behaves differently.

The range of the scaling upon correlation length listed in the forth column in table I. The value of C^*_s denotes the correlation length at small scales and C^*_l for large scales. The higher C^* value represents a smoother surface (as we expected from Fig.3). The correlation length obtained from the structure function is also a measure of minimum lateral size of surface features at each annealing temperature.

The another important WO_3 film parameter is the effective area of the sample which has an important role in the gas sensitivity of WO_3 surfaces. To obtain a measure for this, we utilize the level crossing analysis. As shown in Fig.5, the average frequency ν^+_α as a function of height h, is plotted for the various annealing temperatures. The broad curves indicate the higher magnitude of height fluctuations around the average, and sharp curves show that the most of fluctuations are around the height average. This conclusion is in the correspondence with the results obtained from Fig.3.

According to the Eq.(11) N^+_α i.e. The total number of the crossing surface with positive slope is proportional to the square of area of the growing surface. To obtain the optimum value of the effective area, we have calculated the ratio of effective areas with respect to the area of the "as deposited" surface (27^oC). The values are given

TABLE I: The Roughness exponent, roughness, correlation length and effective area relative to the "as deposited" sample area (27^oC).

T $[^oC]$	$\alpha-\alpha'$	$\sigma[nm]$	C^*_s-$C^*_l\,[nm]$	$N^+/N^+(27^oC)$
27	$0.15-none$	0.91	$60-none$	1.00
200	$0.15-none$	0.98	$60-none$	1.08 ± 0.02
300	$0.61-none$	2.20	$100-none$	1.17 ± 0.02
350	$0.62-none$	11.50	$100-none$	1.67 ± 0.02
400	$0.40-0.15$	17.00	$100-300$	2.00 ± 0.02
450	$0.71-0.20$	30.00	$400-1000$	1.72 ± 0.02
500	$0.69-0.24$	48.00	$200-1400$	1.41 ± 0.02

in the last column in Table I. It means, although the roughness increases by the annealing temperature but the effective square area of the rough surface has a maximum value of N^+_{tot} [27].
For more clarity, we have calculated the temperature dependence of normalized N^+_α numerically (Fig.6) around 400^oC, and we have obtained the three following functions for this quantity :

$$N^+_{tot}(T) = (5.0718 - 0.0223\times T + 2.72\times10^{-5}\times T^2)^{-1} \quad (12)$$

$$ln(N^+_{tot}(T)) = -6.3632 + 0.0344\times T - 4.20\times10^{-5}\times T^2 \quad (13)$$

$$N^+_{tot}(T) = -8.7057 + 0.0520\times T - 6.37\times10^{-5}\times T^2 \quad (14)$$

According to this figure, the maximum value of the effective area is at 400^oC (with respect to its value at 27^oC) with the relative value equal to 2.00. Thus, applying this analysis easily shows that if one follows the condition which the effective area as an important parameter in the gas sensitivity of WO_3 surfaces is optimum and furthermore, the film composition has not been changed (e.g. The Magneli phase transition has not been occurred), should choose the annealed surface at 400^oC for better performance.

V. CONCLUSIONS

We have investigated the role of annealing temperature, as an external parameter, to control the statistical properties of a rough WO_3 surface. The AFM microstructure of the surfaces is just needed to apply in our analysis. We have computed the statistical quantities such as roughness exponent, roughness and lateral size of surface features of the "as deposited" and annealed

surfaces at 200, 300, 350, 400, 450, and 500^oC, using the structure function. We have seen a phase transition at 400^oC, because for higher temperatures there are two sets of roughness parameters, due to structural changes from amorphous to the crystalline phase. Moreover, using the level crossing analysis we have obtained an optimum annealing temperature, 400^oC in which the surface of the WO_3 has maximum value about twice relative to the "as deposited" film without any changes in the film composition that may increase surface reaction of the WO_3 film as the gas sensor or photo-catalyst.

VI. ACKNOWLEDGMENT

GRJ and AAS would like to thank S.M.Fazeli for his useful comments and especially M.R.Rahimitabar for his useful lectures on "stochastic data analysis". AZM would like to acknowledge research council of Sharif University of Technology for financial support of the work.

---

[1] C. G. Granqvist, Handbook of Electrochromic Materials (Elsevier, Amsterdam, 1995).
[2] P. R. Bueno, F. M. Pontes, E. R. Leite, L. O. S. Bulhes, P. S. Pizani, P. N. Lisboa-Filho, and W. H. Schreiner, J. Appl. Phys. 96, 2102 (2004).
[3] R. Azimirad, O. Akhavan, and A. Z. Moshfegh, J. Electrochem. Soc.153, E11(2006).
[4] A. Siokou, S. Ntais, S. Papaefthimiou, G. Leftheriotis, and P. Yianoulis, Surface Science, 566/568, 1168 (2004).
[5] S.-L. Kuai, G. Bader, and P. V. Ashrit, App. Phys. Lett., 86, 221110 (2005).
[6] Y. Takeda, N. Kato, T. Fukano, A. Takeichi, and T. Motohiro, J. Appl. Phys., 96, 2417 (2004).
[7] C. O. Avellaneda and L. O. S. Bulhes, Solid State Ionics, 165, 117 (2003).
[8] S.-H. Lee, H. M. Cheong, P. Liu, D. Smith, C. Edwin Tracy, A. Mascanrenhas, J. R. Pitts, and S.K. Deb, J. Appl. Phys., 88, 3076 (2000).
[9] Y. S. Kim, S.-C. Ha, K. Kim, H. Yang, S.-Y. Choi, Y. T. Kim, J. T. Park, C. H. Lee, J. Choi, J. Paek, and K. Lee, Appl. Phys. Lett., 86, 213105 (2005).
[10] E. Gyrgy, G. Socol, I. N. Mihailescu, C. Ducu, and S. Ciuca, J. Appl. Phys., 97, 093527 (2005).
[11] H. Kawasaki, T. Ueda, Y. Suda, and T. Ohshima, Sens. Actuators B, 100, 266 (2004).
[12] M. A. Gondal, A. Hameed, Z. H. Yamani, and A. Suwaiyan, Chem. Phys. Lett., 385, 111 (2004).
[13] M. Feng, A. L. Pan, H. R. Zhang, Z. A. Li, F. Liu, H. W. Liu, D. X. Shi, B. S. Zou, and H. J. Gao, Appl. Phys. Lett., 86, 141901 (2005).
[14] J. Hao, S. A. Studenikin, and M. Cocivera, J. Appl. Phys., 90, 5064 (2001).
[15] G. Garcia-Belmonte, P. R. Bueno, F. Fabregat-Santiago, and J. Bisquert, J. Appl. Phys., 96, 853 (2004).
[16] M. Seman and C. A. Wolden, J. Vac. Sci. Technol. A, 21, 1927 (2003).
[17] M. Stankova, X. Vilanova, E. Llobet, J. Calderer, C. Bittencourt, J. J. Pireaux and X. Correig, Sens. Actuators B, 105, 271 (2005).
[18] A.L. Barabasi and H.E. Stanley, *Fractal Concepts in Surface Growth* (Cambridge University Press, New York, 1995).
[19] G. R. Jafari, S.M. Fazeli, F. Ghasemi, S.M. Vaez Allaei, M. Reza Rahimi Tabar, A. Irajizad, and G. Kavei, Phys. Rev. Lett. **91**, 226101 (2003).
[20] G. R. Jafari, S. M. Mahdavi, A. Iraji zad, and P. Kaghazchi, Surface And Interface Analysis; 37: 641 645 (2005).
[21] A. Irajizad, G. Kavei, M. Reza Rahimi Tabar, and S.M. Vaez Allaei, J. Phys.: Condens. Matter **15**, 1889 (2003).
[22] T. Halpin-Healy and Y.C. Zhang, Phys. Rep. **254**, 218 (1995); J. Krug, Adv. Phys. **46**, 139 (1997).
[23] J. Krug and H. Spohn "*In Solids Far From Equilibrium Growth, Morphology and Defects*", edited by C. Godreche (Cambridge University Press, New York, 1990).
[24] P. Meakin *Fractals, Scaling and Growth Far From Equilibrium* (Cambridge University Press, Cambridge, 1998).
[25] M. Kardar, Physica A **281**, 295 (2000).
[26] A.A. Masoudi, F. Shahbazi, J. Davoudi, and M. Reza Rahimi Tabar, Phys. Rev. E **65**, 026132 (2002).
[27] P. Sangpour, G. R. Jafari, O. Akhavan, A.Z. Moshfegh, and M. Reza Rahimi Tabar, Phys.Rev.B 71, 155423 (2005).
[28] F. Shahbazi, S. Sobhanian, M. Reza Rahimi Tabar, S. Khorram, G.R. Frootan, and H. Zahed, J. Phys. A **36**, 2517 (2003).
[29] M. Sadegh Movahed, A. Bahraminasab, H. Rezazadeh, A. A. Masoudi, cond-mat/0509077 (2005).
[30] A. Bahraminasab, M. Sadegh Movahed, S. D. Nassiri and A. A. Masoudi, cond-mat/0508180 (2005).
[31] G. R. Jafari, M. S. Movahed, S. M. Fazeli, M. Reza Rahimi Tabar, and S. F. Masoudi, Jstat. Mech. P06008, (2006).
[32] A. Z. Moshfegh, R. Azimirad, and O. Akhavan, Thin Solid Films, 484, 124 (2005).
[33] B. V. Crist, Handbook of Monochromatic XPS Spectra: The Elements and Native Oxides, Vol. 1 (John Wiley & Sons Ltd, Chichester, 2000).
[34] K. D. Lee, Thin Solid Films, 302, 84 (1997).
[35] M. D. Antonik, J. E. Schneider, E. L. Wittman, K. Snow, J. F. Vetelino, and R. J. Lad, Thin Solid Films, 256, 247 (1995).
[36] A. Al-Mohammad and M. Gillet, Thin Solid Films, 408, 302 (2002).